CRYSTAL GROWTH & DESIGN

Article

Investigating the solubilities of the nitrate and isomorphous bromide and chloride salts of dapsone

Cristiane Cabral de Melo, Monalisa Bitencourt, Charlane C. Corrêa, and Antonio C. Doriguetto

Cryst. Growth Des., **Just Accepted Manuscript** • DOI: 10.1021/acs.cgd.9b01467 • Publication Date (Web): 20 Feb 2020

is published by the American Chemical Society. 1155 Sixteenth Street N.W., Washington, DC 20036

Investigating the Solubilities of the Nitrate and Isomorphous Bromide and Chloride Salts of Dapsone

Cristiane Cabral de Melo[*†,‡], *Monalisa Bitencourt*[†], *Charlane C. Corrêa*[§], *Antonio C. Doriguetto*[*†,‡]

[†]Faculty of Pharmaceutical Sciences and [‡]Institute of Chemistry, Federal University of Alfenas, 37130-001, Alfenas-MG, Brazil

[§]Department of Chemistry, Federal University of Juiz de Fora, 36036-900, Juiz de Fora-MG, Brazil

*Corresponding authors: doriguetto@unifal-mg.edu.br; crisbrizoti@gmail.com

ABSTRACT. Dapsone, the major drug for leprosy, has broader application against dermatoses, malaria and AIDS-related diseases. Besides its antimicrobial/antiprotozoal activity, dapsone has anti-inflammatory properties. However, because of its low aqueous solubility, the high oral doses required and associated side effects limit the tolerability and efficacy of dapsone free base. As a strategy to improve the drug's solubility, new salts of dapsone were prepared. The chloride, bromide and nitrate salts of dapsone were completely characterized by X-ray diffraction (single and powder), spectroscopic (FT-IR) and thermal (DSC and TGA) techniques. The X-ray results revealed that dapsone chloride and dapsone bromide are isomorphous compounds. Dapsone salts decompose without melting and are thermally less stable than dapsone free base. The equilibrium solubility of dapsone salts was

compared to dapsone free base in three aqueous media: HCl buffer pH 1.2, acetate buffer pH 4.5 and phosphate buffer pH 6.8. The highest solubility values were obtained in acid media and dapsone bromide was found to be slightly more soluble than dapsone free base. The solubility values obtained for the nitrate and chloride salts of dapsone at pH 1.2 cannot be considered real, since the PXRD patterns show their total/partial conversion.

Keywords: Leprosy, dapsone salts, isomorphism, thermal behavior, solubility.

1. INTRODUCTION

One of the most important parameters in the process of drug design and pharmaceutical development, especially for oral-drug delivery systems, is solubility.[1] The extensive use of combinatorial chemistry with high-throughput screening has brought a great number of drugs with poor solubility into development.[2] Together with low permeability, poor solubility is the main factor behind the incomplete absorption of a drug and therefore of its low or erratic bioavailability.[1,2] To improve drug solubility, several physical or chemical methods have been used including the reduction of particle size by milling or nanosuspensions, the use of solubilizing excipients, complexation with cyclodextrins and salt formation, the latter being most commonly used for drugs containing ionizable groups.[1–5] It is well known, and well documented, that a salt can be prepared in accordance with the ΔpK_a rule.[6] Although not formally proven, the ΔpK_a rule establishes that when the pK_a difference between the salt former and the drug is greater than 2 or 3 (pK_a[protonated base] - pK_a[acid] > 2 or 3), salt formation is expected.[6]

Dapsone (4,4'-diaminodiphenyl sulfone, DDS ─ **Scheme 1)** is a synthetic antibiotic introduced in the 1940s as a monotherapy for the treatment of *Mycobacterium leprae*.[7,8] Like other sulfone drugs, dapsone's mechanism of action involves the interruption of folic acid synthesis (essential for DNA and RNA synthesis) by inhibition of the bacterial enzyme dihydropteroate synthase. However, among the sulfone drugs, DDS is the only one which is effective against *M. leprae.*[7] Currently, leprosy treatment with dapsone alone is contraindicated and a multi-drug therapy, by combination of dapsone, rifampicin and clofazimine, should be adopted according to the World Health Organization (WHO) regimen.[9] Because of its low water solubility (0.2 $mg.mL^{-1}$) and high toxicity, other supramolecular solid forms of DDS, such as salts and cocrystals, have recently been investigated.[8]

DDS is a very weak Lewis base able to form either salts or cocrystals. DDS contains two ionizable amine groups and can therefore form a monosalt or a disalt compound. The first acid constant has a pK_a of 2.49 for the equilibrium between ammonium (H_3N^+-aryl) and the neutral form (H_2N-aryl) and the second has a pK_a of 1.30 (monosalt-disalt equilibrium).[10] It is curious that besides the potential for salt formation, few salt structures of DDS are known (eight X-ray structures) and only two have pharmaceutical relevance (the mesylate monohydrate and the nitrate hemihydrate).[11–15] A search for crystallographic forms of DDS in the Cambridge Structural Database (CSD, v. 5.40, November 2018, update 1, Feb 2019) returned five polymorphs, one hydrate (with the unusual DDS: water stoichiometry of 3:1), four solvates with dichloromethane (being two polymorphs), dioxane and tetrahydrofuran and 12 cocrystals besides the salts structures.[16–20]

Considering that DDS is a BCS Class II drug, our main interest is the development of thermally stable and highly soluble DDS salts.[21] We chose three acids (HCl, HBr and HNO_3) belonging to the GRAS (generally recognized as safe) category in order to incorporate these features, and also to synthesize pharmaceutically-acceptable crystalline salts.[22] Unfortunately,

during the course of our experiments, the single-crystal X-ray structure of the nitrate salt was published.[23] Even so, we decided to keep the nitrate salt for comparative purposes and here we also report, for the first time, the crystal structure of DDS bromide and DDS chloride forms. The DDS salts were completely characterized using Fourier Transform Infrared Spectroscopy (FT-IR), Thermogravimetric Analysis (TGA), Differential Scanning Calorimetry (DSC) and Powder X-ray Diffraction (PXRD) techniques. Finally, this study also presents the equilibrium solubility of DDS and DDS salts in three different aqueous media.

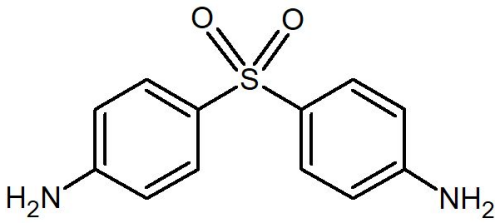

Scheme 1. Molecular structure of Dapsone

2. EXPERIMENTAL SECTION

2.1 Samples. DDS was purchased from Sigma-Aldrich Brazil® and used as received. The solvents (HPLC grade) and the chloride, bromide and nitric acids were obtained from commercial sources and used as received.

2.2 Synthesis. DDS chloride, DDS bromide and DDS nitrate were prepared by adding 2.0 mL of the corresponding concentrated acid into a saturated ethanolic solution of DDS (20 mL). The precipitated solid was filtered and recrystallized from an aqueous methanol solution.

2.3 Single crystal X-ray Diffraction. A suitable single crystal of each DDS salt was selected for processing. Data collection was performed on an Agilent SuperNova diffractometer, equipped with a dual source of radiation (Cu and Mo) and an Atlas S2 CCD detector, at room temperature (293 K for DDS bromide and nitrate salts) or low temperature (200 K for DDS chloride). The data collection routine, unit cell determination and intensity

data integration were carried out using CrysalisPro software.[24] The structures were solved by direct methods and refined by full-matrix least-squares on F^2 using SHELXL-2018/3.[25] The non-hydrogen atoms were refined anisotropically. The hydrogen atoms were placed in idealized positions and refined using a rigid model, constraining their isotropic displacement parameters to be equal to 1.2 or 1.5 times the corresponding isotropic displacement parameters of the bonded atom. The MERCURY (version 3.9) program was used to prepare the artwork representations for publication.[26] The CIFs of these three structures were deposited in the Cambridge Structural Data Base under the codes CCDC 1963117, CCDC 1963118 and CCDC 1963119.[27] Copies of these files may be solicited free of charge via www.ccdc.cam.ac.uk, by emailing data_request@ccdc.cam.ac.uk or by contacting The Cambridge Crystallographic Data Centre, CCDC, 12 Union Road, Cambridge CB2 1EZ, UK; Fax + 44 1223-336033.

2.4 Powder X-ray Diffraction (PXRD). To check the authenticity, all samples (DDS and its salts), as well as the solid residues from the equilibrium solubility measurements, were subjected to PXRD analysis. The polycrystalline samples were powdered and mounted onto a sample holder. The milled samples were analyzed using a Rigaku Ultima IV powder diffractometer with the following experimental conditions: CuKα radiation, λ = 1.5418 Å; 40 kV; 30 mA; step scan with a step width of 0.02° over an interval of 3°– 35° in 2θ; time per step 3s.

2.5 Thermal Analysis. TGA was performed on a TA Instruments Q600. Approximately 10.0 mg of each sample was placed in an open alumina pan and heated from ambient (≈25 °C) to 400 °C at a constant rate of 10 °C.min^{-1} under a N_2 flow (50 mL.min^{-1}). A TA Instruments Q100 model was used to produce DSC curves. The samples (≈3.00 mg) were heated from room temperature (≈30 °C) to the beginning of the decomposition process at a constant rate of 10 °C.min^{-1} in a closed aluminum pan. The purge gas was N_2 under a flow of 50 mL.min^{-1}.

2.6 Fourier Transform Infrared spectroscopy (FT-IR). The spectra were recorded on a Shimadzu IR Prestige-21 spectrophotometer, using KBr pellets, in the range of 4000–400 cm^{-1}, with an average of 64 scans and 4 cm^{-1} resolution.

2.7 Equilibrium solubility studies. DDS solubility was determined in three different aqueous media (HCl buffer pH 1.2, acetate buffer pH 4.5 and phosphate buffer pH 6.8) using the traditional shake-flask method. The concentrations of DDS and DDS salts were determined by the UV-Vis method (Shimadzu™ UV-Vis spectrophotometer, model UV-1800) using a DDS calibration curve at concentration range 4–13 $\mu g.mL^{-1}$ (Electronic Supplementary Information, Figure S1). In all media, DDS and DDS salts showed absorbance maxima at 295 nm (Figure S2). DDS and DDS salts were put into a beaker containing 65 mL of each dissolution media separately, until saturation was reached (a deposit of DDS free base and DDS salts not solubilizing). The experiment was performed in triplicate and at room temperature (25 ±2 °C). The beakers were covered and protected from the light and agitated at 150 rpm using an orbital shaker, Marconi model MA-830/A (Marconi™, Piracicaba, SP – Brazil). After 48 h of stirring, the solutions were filtered through a 0.45 μm pore-size 25 mm PTFE syringe filter and diluted when necessary in the corresponding medium for further UV-Vis analysis. The pH variation in each dissolution medium (Table S2, Supplementary Information Section) was analyzed using a pH meter, Marconi model PA 200 (Marconi™, Piracicaba, SP – Brazil).

3. RESULTS AND DISCUSSION

3.1 Structural Description. The asymmetric units of DDS chloride, DDS bromide and DDS nitrate are shown in Figure S3 with their respective labels. Their crystallographic data are summarized in Table 1. A diprotonated DDS cation occurs in all the salts, since the two nitrogen amino atoms (N1 and N2) are protonated. The sulfone group in the DDS cations assumes a distorted tetrahedron configuration. The large deviation of the angle O1=S1=O2

(119.9(1)^o for chloride, 119.6(2)^o for bromide and 119.7(2)^o for nitrate) from the ideal tetrahedron value of 109.47^o is an intrinsic characteristic of the sulfones and can be attributed to the involvement of the 3*d*-orbitals of sulfur in the bonding.[28] For DDS free base, including its hydrates and polymorphs, this angle varies from 117.4(1)° (CCDC code: ANSFON02) to 120.6(9)° (CCDC code: TUXDEW). Dapsone molecules can exist in different conformations because of their free rotation around the C1-S1 and S1-C7 bonds. In dapsone nitrate, two torsion angles define the cation conformation: C6-C1-S1-C7 = 94.0(3)° and C8-C7-S1-C1 = 92.1(2)°. In the bromide and chloride salts, the conformation is defined by the C6-C1-S1-C1' torsion angle, which assume the values of 97.0(3)° and 85.1(2)°, respectively.

Table 1. Crystal data and structure refinement parameters for DDS salts

SALT	**DDSNO$_3$**	**DDSBr**	**DDSCl**
Crystal data			
Formula	$C_{12}H_{14}N_2O_2S^{2+}.2NO_3^-$	$C_{12}H_{14}N_2O_2S^{2+}.2Br^-$	$C_{12}H_{14}N_2O_2S^{2+}.2Cl^-$
Formula weight (g.mol^{-1})	374.33	410.11	321.22
Wavelength (Å)	0.71073	0.71073	0.71073
Crystal System	Orthorhombic	Orthorhombic	Orthorhombic
Space group	*P*na2$_1$	*P*nma	*P*nma
Temperature (K)	293	293	200
Unit cell dimensions			
a (Å)	7.6701(4)	9.4169(6)	9.2724(5)
b (Å)	9.0611(5)	25.5794(16)	25.0339(14)
c (Å)	21.8546(12)	5.9945(4)	5.8561(4)
Volume (Å^3)	1518.88(14)	1443.95(16)	1359.34(14)
Z, Z'	Z: 4, Z': 1	Z: 8, Z': ½	Z: 8, Z': ½
μ (mm^{-1})	0.268	5.757	0.629
Absorption correction	multi-scan	multi-scan	multi-scan
Tmax, Tmin	1.000, 0.314	0.178, 0.044	1.000, 0.630
Crystal size (mm)	0.4 x 0.3 x 0.3	0.9 x 0.5 x 0.3	0.6 x 0.5 x 0.2
Data collection			
Diffractometer	SuperNova, AtlasS2	SuperNova, AtlasS2	SuperNova, AtlasS2
R_{int}	0.0462	0.0741	0.0407
$(\sin\theta/\lambda)_{max}$ (Å^{-1})	0.703	0.694	0.7163

No. of measured, independent and observed [I >2σ(I)] reflections	31312, 4096, 3577	11304, 1954, 1390	8092,1785, 1529
Refinement			
No. of reflections	4096	1954	1785
No. of parameters	228	92	92
No. of restraints	1	0	0
Goodness-of-fit on F^2	1.026	1.068	1.070
R [I >2σ(I)]	R1 = 0.0384, wR2 = 0.0881	R_1 = 0.0471, wR_2 = 0.0996	R_1 = 0.0376, wR_2 = 0.0905
R (all data)	R1 = 0.0481, wR2 = 0.0948	R_1 = 0.0761, wR_2 = 0.1148	R_1 = 0.0461, wR_2 = 0.0963
$\Delta\rho_{max}$, $\Delta\rho_{min}$ (e Å^{-3})	0.17, -0.24	0.808, -0.776	0.312, -0.472

The chloride and bromide salts are isomorphous compounds that crystallize in the orthorhombic space group *P*nma, with the sulfur and oxygen atoms of the drug located on a crystallographic plane of symmetry, and, therefore, their asymmetric unit consists of one-half dapsone cation and one bromide anion. The packing analysis shows that DDS molecules are stabilized by charge-assisted H-bonds (CAHBs) involving the protonated amino N1 atom of the drug and the corresponding anion (Table S1). Each anion (Cl^- or Br^-) is attached to two DDS molecules, related by inversion, via N1-H1B···Cl/Br (D···A = 3.344(2)/3.301(3) Å) and N1-H1C···Cl/Br (D···A = 3.122(2)/3.305(3) Å) CAHBs (Figure 1).

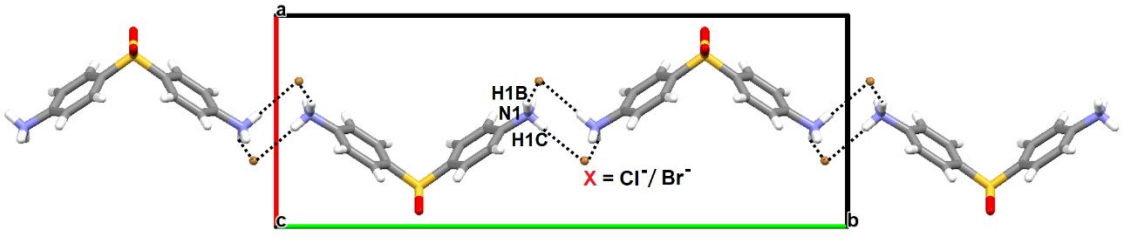

Figure 1. View of the isomorphous 1D chains of DDS chloride and DDS bromide salts along the [010] direction

The combination of these interactions leads to the formation of a ring motif $R_4^2(8)$[29] along the crystallographic [010] direction (Figure 2). This hydrogen bonded motif propagates

along the c-axis by unit cell translations to form one-dimensional pleated sheets that are also stabilized by CAHBs (N1-H1A···Cl/Br, D···A = 3.160(2)/3.458(3) Å) and, as a result, a fused $R_4^2(8)$ motif is formed along the [001] direction (Figure 2). The 3D-assembly is characterized by the stacking of these sheets along the [100] direction through van der Waals contacts (Figure S4).

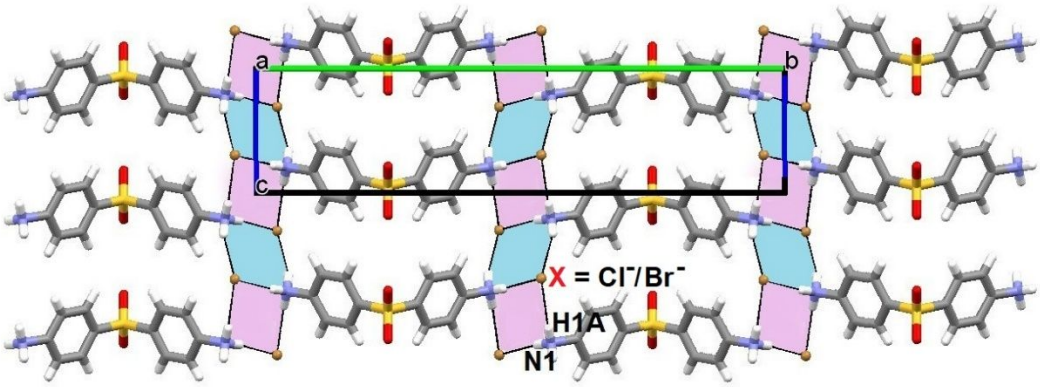

Figure 2. Pleated sheet structures in the *bc* plane of the isomorphous DDS chloride and DDS bromide salts

.

In contrast to the chloride and bromide salts, DDS nitrate crystalizes in the orthorhombic space group *P*na2$_1$ with two nitrate anions and one DDS dication in the asymmetric unit. As the nitrate anion is a conjugate base of a monoprotic acid (HNO_3), the 1:2 stoichiometry is necessary to allow the double protonation of DDS, where two acid molecules transfer their protons to both amine groups of the drug.

The drug molecules propagate along the [001] direction by stronger two- and three-center hydrogen bonds involving their protonated amine groups and the nitrate anions (Figure 3a). One of the nitrates acts as a bridge, connecting two crystallographic symmetry-related cations (related by a 2$_1$-screw axis) through three CAHBs with distances from donor (N1 and N2

atoms) to acceptor (O6, O7, O8 atoms) ranging from 2.8 to 3.3 Å (see Table S1, Figure 3b). The presence of the screw axis (parallel to the c-axis) and, consequently, of these interactions leads to the formation of infinite helical chains along the [001] direction (Figure 3a). Here, also, the nitrate anions serve as a link for the helical chains via the bifurcated three-center hydrogen bonds. The 2D layer (helix-bound layer) lies parallel to the (100) plane and is stabilized by the following CAHBs: N1-H1C···O4 (D···A = 3.005(4) Å), N1-H1C···O5 (D···A = 2.909(4) Å), N2-H2C···O5 (D···A = 2.839(4) Å) and N2-H2C···O3 (D···A = 3.117(4) Å) (Figure 3c).

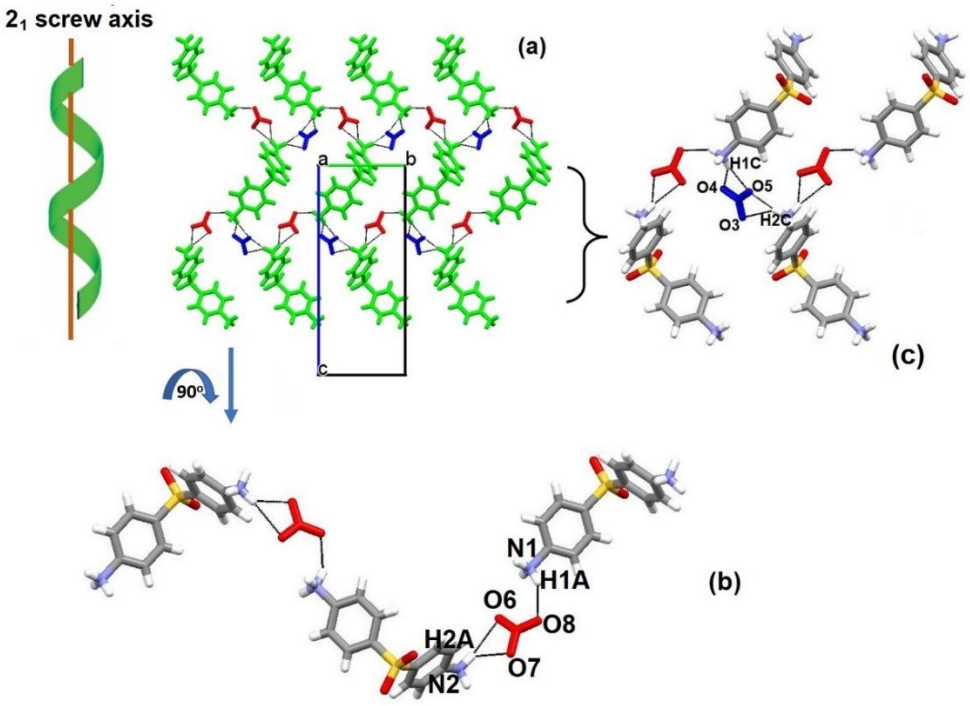

Figure 3. Packing view of the helical chains (layer A) of DDS nitrate along the *bc* plane (a). Representation of the helical chain unit (b). Partial view of layer A highlighting the nitrate interactions (c).

When viewed along the [100] direction, the 3D assembly can be described by two types of layers, A and B. In fact, since they are related by symmetry, both layers display the same pattern of interactions. The A and B helices (or layers) run in opposite directions and

Figure 4. Assembly of type A (right-handed) and type B (left-handed) helical chains. They interweave through CAHB and non-classical C-H···π and π···π hydrogen bonds.

interweave via N1-H1B···O7 (D···A = 2.702(4) Å) CAHB and non-classical C2-H2···π and π···π hydrogen bonds (Figure 4). The overall 3D structure is characterized by the assembling of these layers in an "…A-B-A-B…" fashion along the [100] direction (Figure 5). Additionally, the ···A-A-A··· and ···B-B-B··· helices are also connected to one another along the [100] direction through a hydrogen bond involving the sulfonyl oxygen and one of the protonated amine groups of the drug (N2-H2B…O1, D···A = 3.023(4) Å) (Figure S5).

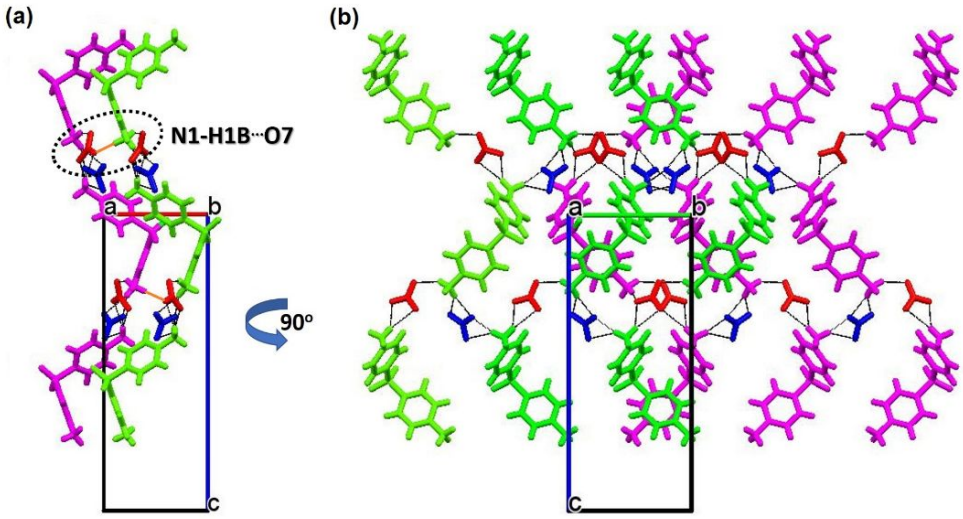

Figure 5. Representation of the double helical structure. View along the [010] (a) and [100] (b) directions.

3.2 Thermal and FT-IR results. The TG/DTG/DSC curves of DDS free base and DDS salts are presented in Figure 6. The DSC curve of DDS is characterized by two endothermic peaks, one at 81.0 °C and the other one at 180.1 °C. The first peak is ascribed to a polymorphic transition of DDS[17], whereas the second is due to the melting of DDS (polymorph I). This result is in good agreement with the TG curve, since the sample did not undergo any weight loss in the interval of 30–190 °C. The TG shows that DDS is stable up to an onset temperature of 353.8 °C; above this temperature, the TG curve is characterized by an abrupt weight loss as the result of thermal decomposition. The first weight loss for the DDS salts is observed below

353.8 °C, which shows that they are thermally less stable than DDS. Of the salts analyzed, the nitrate and chloride are least stable, with an onset temperature of 149.2 °C and 151.5 °C, respectively, followed by the bromide (T_{onset} = 232.3 °C) salt. In contrast to DDS, the salts do not show a DSC peak that could be attributed to melting; in fact, the first endotherms appear after the beginning of thermal decomposition, i.e. after the onset temperatures extracted from the TG curves.

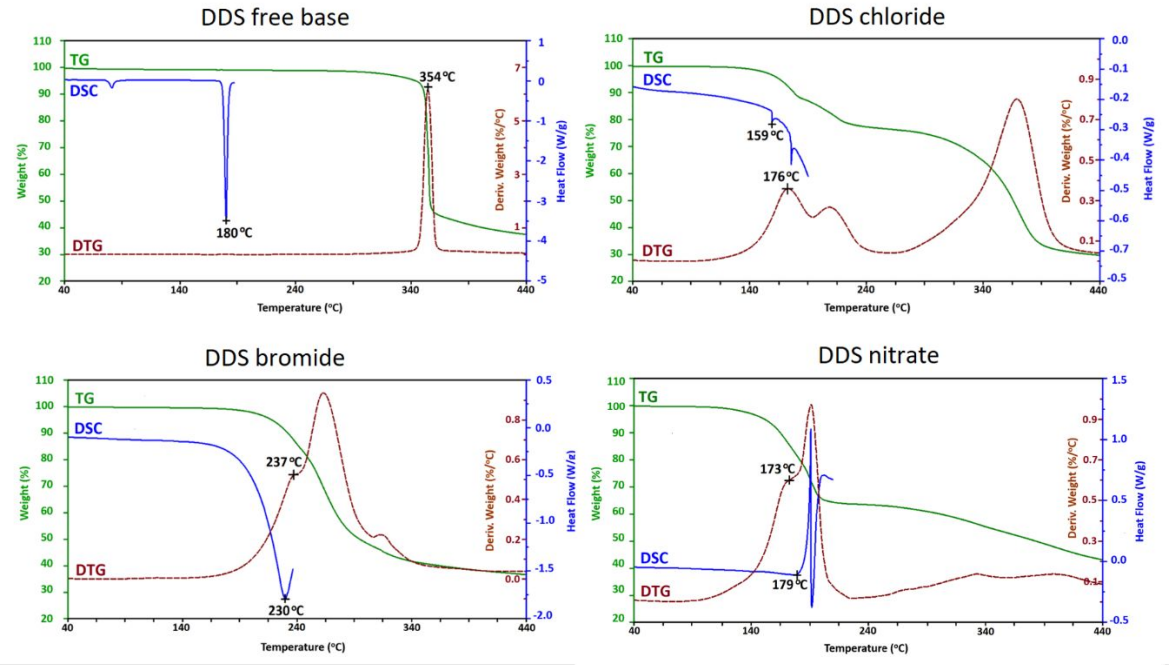

Figure 6. TG/DTG/DSC curves of DDS free base and DDS salts under N_2 flow.

FT-IR not only provides information about the molecular conformation, but is also a powerful and low-cost method of monitoring salt formation.[30] Figure 7 presents the FT-IR spectrum of DDS free base as well as the DDS salts, using KBr pellets. The main changes are observed in the region 3500–2500 cm^{-1}. The observed bands are assigned in accordance with data available in the literature, i.e., the experimental and calculated spectra of DDS and protonated primary amines.[30–32] The absorptions associated with the drug's amine groups are

essential to distinguish between a protonated and neutral species. The DDS spectrum is characterized by a series of bands in the region 3460–3340 cm^{-1} (bands at 3455, 3397, 3369 and 3341 cm^{-1}) related to the antisymmetric and symmetric NH_2 stretching modes. The conversion of NH_2 into NH_3^+ (the salt formation) results in the absence of these bands (suppressed or shifted/overlapped) and the emergence of a set of broad bands in a lower frequency range (3100–2500 cm^{-1}) associated with the antisymmetric and symmetric NH_3^+ stretches and to the combination modes and overtones of the bending and rocking vibrations of NH_3^+.

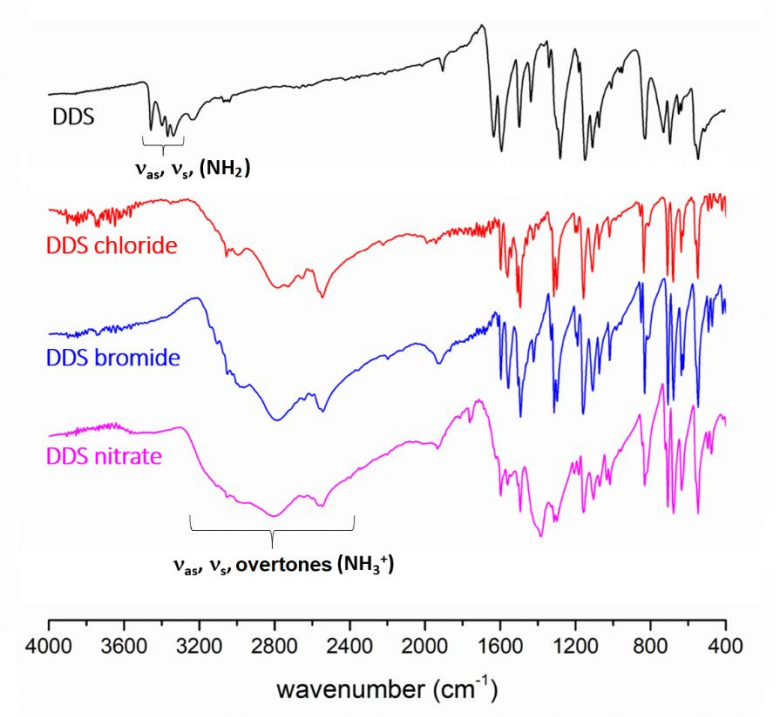

Figure 7. FT-IR spectra of DDS free base and DDS salts in KBr pellets.

3.3 Characterization of DDS salts from the bulk. PXRD (Figure 8) was used not only as an additional technique to monitor the salt formation but also to ensure that the single-crystal structure is representative of the bulk obtained by acid precipitation. The experimental diffractograms of DDS salts are in good agreement with those calculated by the Mercury

program, using as input the corresponding single-crystal salt structures: DDS chloride (CCDC code: 1963117), bromide DDS (CCDC code: 1963118) and DDS nitrate (CCDC code: 1963119). The match between the experimental and calculated Bragg peaks confirms the complete conversion of DDS free base into the salts and the yield of the preparation process.

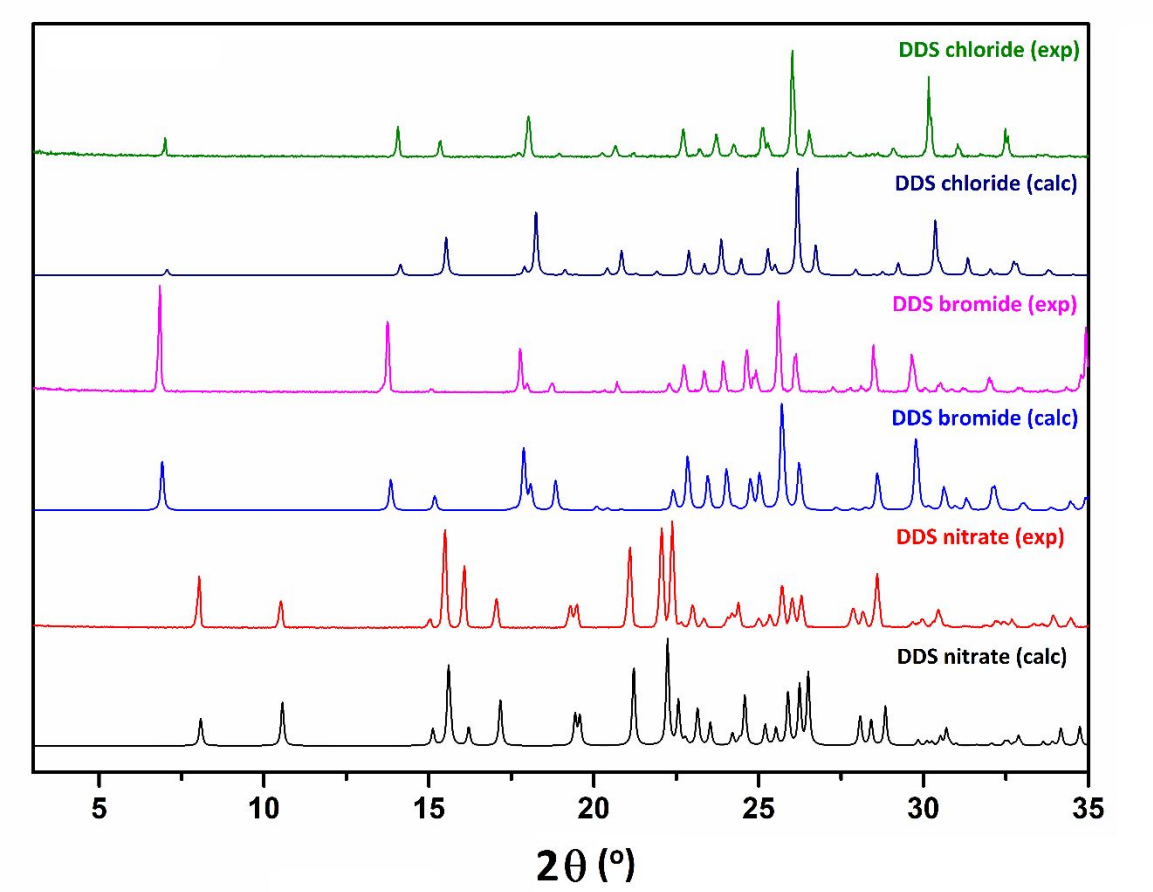

Figure 8. Experimental and calculated PXRD patterns of DDS salts.

3.4 Equilibrium solubility studies. The pH-solubility profile of DDS and DDS salts in three different pH conditions (pH 1.2, pH 4.5 and pH 6.8) is shown in Figure 9. This range was chosen in order to mimic the acidic gastric medium (HCl buffer pH 1.2) and biological fluids (acetate buffer pH 4.5 and phosphate buffer pH 6.8). The equilibrium pH values were measured after the addition of each DDS form and at the end of the equilibrium solubility experiment (Table S2), and they did not show any significant difference.

According to the results obtained for pH 4.5 and pH 6.8 (Table 2), the solubility of DDS and DDS salts is less than 0.500 mg.mL^{-1}. At pH 4.5, the solubility of DDS free base is slightly higher (0.264 ±0.004 mg.mL^{-1}) than that of DDS chloride (0.203 ±0.001 mg.mL^{-1}), DDS bromide (0.079 ±0.001 mg.mL^{-1}) and DDS nitrate (0.072 ±0.001 mg.mL^{-1}) salts. Also, at pH 6.8 solubility values remain significantly low: 0.167 ±0.001 mg.mL^{-1} for DDS chloride, 0.108 ±0.002 mg.mL^{-1} for DDS bromide, 0.091 ±0.031 mg.mL^{-1} for DDS free base and 0.075 ±0.001 mg.mL^{-1} for DDS nitrate. The lower solubility at this pH range can be explained by a possible conversion of the cationic DDS species to its neutral form, i.e. DDS free base ($DDS^{0}_{(sol)}$), which is practically insoluble in these media. Since DDS is a weak dibasic compound, its dissolution and solubility depend on the ionization state that in turn is controlled by the pH of the medium and the dissociation constant (pK_a). As explained in the Introduction, DDS has two pK_a values, where pK_{a1} (2.49) is associated with the monosalt-neutral equilibrium ($DDSH^{+}_{(sol)} \leftrightarrow DDS^{0}_{(sol)} + H^{+}$) and p$K_{a2}$ (1.30) with the monosalt-disalt equilibrium ($DDSH^{2+}_{2(sol)} \leftrightarrow DDSH^{+}_{(sol)} + H^{+}$). Therefore, taking into account the calculated pH-dependent acid-base DDS species distribution (insert in Figure 9), the molar fraction of the less soluble $DDS^{0}_{(sol)}$ species will be higher in the alkaline pH range than the more soluble $DDSH^{+}_{(sol)}$ species, and *vice versa* in the acidic pH range, where the molar fraction of the $DDSH^{+}_{(sol)}$ will predominate over the $DDS^{0}_{(sol)}$ species. Further, this conversion was confirmed by the PXRD analysis of the solid phase in equilibrium with the saturated solutions used for measuring the solubility (Figure S6). The PXRD patterns from the solid residues at pH 4.5 and pH 6.5 clearly show the presence of peaks intrinsic to the DDS free base pattern.

The highest solubility values are observed for DDS chloride (6.750 ±0.031 mg.mL^{-1}), followed by DDS bromide (3.669 ±0.057 mg.mL^{-1}), DDS nitrate (3.375 ±0.013 mg.mL^{-1}) and DDS free base (2.992 ±0.085 mg.mL^{-1}) in HCl buffer pH 1.2. However, the values obtained

for DDS nitrate and DDS chloride cannot be considered to be real, since the PXRD patterns show their total/partial conversion of them to the non-stoichiometric hydrate of DDS (Figure S7). Nevertheless, DDS bromide salt was found to be slightly more soluble than DDS free base.

Table 2. Equilibrium solubility values $(mg.mL^{-1})$ for DDS free base and DDS salts in three different conditions. The initial pH (pH_i) and final pH (pH_f) pH at the equilibrium of each solution are also given

	DDS free base	DDS chloride	DDS bromide	DDS nitrate
HCl buffer pH 1.2	2.992 ± 0.085 pH_i = 1.20 pH_f = 1.45	6.750 ± 0.031 pH_i = 1.20 pH_f = 1.30	3.669 ± 0.057 pH_i = 1.20 pH_f = 1.50	3.375 ± 0.013 pH_i = 1.20 pH_f = 1.38
Acetate buffer pH 4.5	0.264 ± 0.004 pH_i = 4.55 pH_f = 4.48	0.203 ± 0.001 pH_i = 4.55 pH_f = 4.45	0.079 ± 0.001 pH_i = 4.55 pH_f = 4.16	0.072 ± 0.001 pH_i = 4.55 pH_f = 4.30
Phosphate buffer pH 6.8	0.091 ± 0.031 pH_i = 6.87 pH_f = 6.95	0.167 ± 0.001 pH_i = 6.87 pH_f = 6.80	0.108 ± 0.002 pH_i = 6.87 pH_f = 6.56	0.075 ± 0.001 pH_i = 6.87 pH_f = 6.86

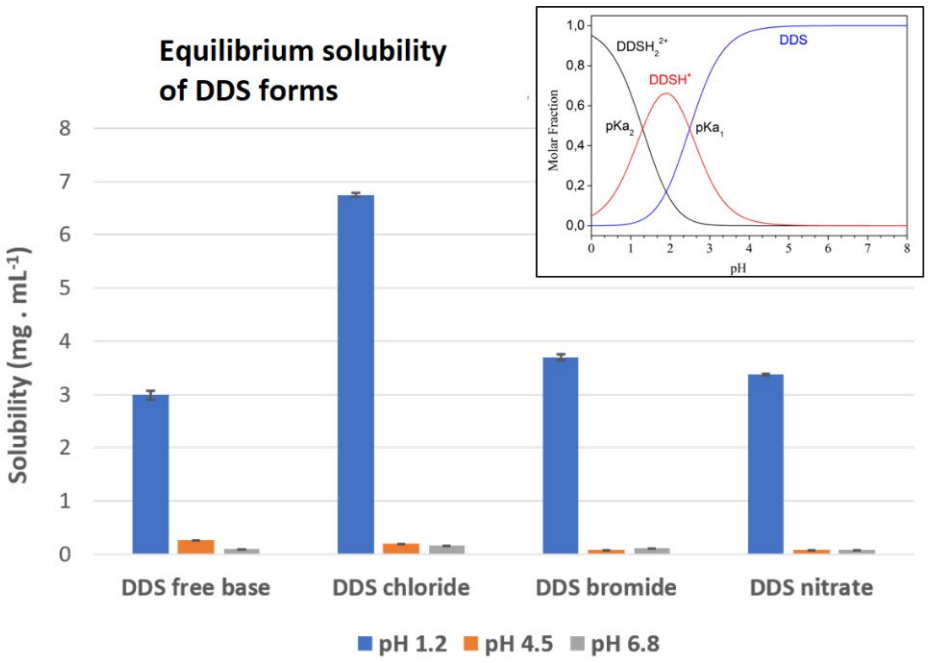

Figure 9. pH-dependent equilibrium solubility values of DDS free base and DDS salts in HCl buffer pH 1.2, acetate buffer pH 4.5 and phosphate buffer pH 6.8.

4. CONCLUSION

In this study, we present the solubility behavior, in three different pH conditions (pH 1.2, pH 4.5 and pH 6.8), of three salts of the anti-leprosy drug DDS compared with DDS free base, the marketed form, followed by a complete solid-state investigation of these salts. The chloride, bromide and nitrate salts were obtained by acid precipitation, whereas the single-crystals were obtained by the slow evaporation method, in which, for the first time, the single-crystal X-ray structures of the isomorphous DDS chloride and DDS bromide salts were determined. Their packing is stabilized by CAHBs between the protonated DDS amino groups and the respective counterions (Cl^-/Br^-), generating a pleated sheet structure. In contrast to DDS free base, which melts at 180.1 °C (T_{peak}), the salts decompose without melting; the nitrate (T_{onset} = 149.2 °C) and the chloride (T_{onset} = 151.5 °C) are less thermally stable, i.e. they are the

salts with the lowest onset temperatures, followed by the bromide salt (T_{onset} = 232.3 °C). The FT-IR and PXRD analysis was congruent with the SCXR results, from the FT-IR it is possible to confirm the salt formation and from the PXRD, to confirm the isomorphism. DDS salts were found to be converted into DDS free base in the slightly alkaline-neutral pH range (pH 4.5 to pH 6.8), which explains their low equilibrium solubility values. The highest values were obtained in acid medium (pH 1.2) in which DDS bromide (3.669 ±0.057 $mg.mL^{-1}$) was a little more soluble than DDS free base (2.992 ±0.085 $mg.mL^{-1}$). For the nitrate and chloride salts, the PXRD patterns of the solid residues showed the appearance of new peaks corresponding to another crystalline form, the non-stoichiometric hydrate of DDS. Therefore, this total/partial conversion in acid medium renders the equilibrium solubility results artificial and not adequate for subsequent (comparative) solubility analyses.

ASSOCIATED CONTENT

Electronic supplementary information (ESI). Figure S1. Calibration curve using standard solutions of DDS; **Figure S2.** UV-Vis spectra of DDS free base and DDS salts in three different conditions; **Figure S3.** ORTEP view of the asymmetric unit of DDS salts: the isomorphous chloride and bromide (a) and the nitrate (b) salts. Thermal ellipsoids for non-hydrogen atoms are drawn at 50% probability level; **Figure S4.** Crystal packing of the isomorphous DDS chloride and DDS bromide salts. The 3D assembly is characterized by the stacking of sheets along the [100] direction; **Figure S5.** A partial view of DDS nitrate packing. The helical layers

A (green) and B (pink) are connected along the [100] direction by nitrate-drug (N1-H1B···O7) and drug-drug (N2-H2B···O1) hydrogen bonds; **Figure S6.** PXRD data of the solid residues from the equilibrium solubility assays of DDS salts and DDS free base in three different media (HCl buffer pH 1.2, acetate buffer pH 4.5 and phosphate buffer pH 6.8). C refers to the control, i.e. the PXRD of the salt used in the solubility assays; **Figure S7.** PXRD data of the solid residues corresponding to the equilibrium solubility of DDS nitrate and DDS chloride at pH 1.2. Both diffractograms show the presence of characteristic peaks related to the non-stoichiometric hydrate form of DDS (CSD code ANSFON02). For DDS nitrate, it was also included the calculated PXRD pattern of the mono-protonated salt (CSD code WINFIL). Unfortunately, there is no structure available for the mono-protonated form of DDS chloride**;** **Table S1.** Geometric parameters of the hydrogen bonds in DDS salts.

Accession Codes

CCDC codes 963117, 963118 and 963119 contain the supplementary crystallographic data for this paper. These data can be obtained free of charge via www.ccdc.cam.ac.uk/getstructures, or by emailing data_request@ccdc.cam.ac.uk, or by contacting The Cambridge Crystallographic Data Centre, 12, Union Road, Cambridge CB2 1EZ, UK; fax: +44 1223 336033.

AUTHOR INFORMATION

Corresponding author

*(A.C.D.) E–mail: doriguetto@unifal-mg.edu.br
*(C.C.M.) E–mail: crisbrizoti@gmail.com

Notes

The authors declare no competing financial interest.

ACKNOWLEDGMENT

This study was financed in part by the Coordenação de Aperfeiçoamento de Pessoal de Nível Superior – Brasil (CAPES) – Finance Code 001 (C.C.M. and M.B.). Other funding for this research was provided by FINEP, CNPq (A.C.D. grants 308162/2015-3 and 428475/2018-3) and FAPEMIG (A.C.D. grants PPM-00533-16 and APQ-01835-18) agencies. The authors express sincere thanks to NCQ-UNIFAL-MG and LABIQ-UNIFAL-MG for the HPLC, TG/DSC and FTIR facilities.

REFERENCES

1. Savjani, K. T.; Gajjar, A. K.; Savjani, J. K. Drug Solubility: Importance and Enhancement Techniques. *ISRN Pharm.* 2012, *2012*, 1–10. https://doi.org/10.5402/2012/195727

2. Lipinski, C. A. Drug-like properties and the causes of poor solubility and poor permeability. *J. Pharmacol. Toxicol. Methods.* 2000, *44*, 235–249. https://doi.org/10.1016/S1056-8719(00)00107-6

3. Kalepu, S. and Nekkanti, V. Insoluble drug delivery strategies: review of recent advances and business prospects. *Acta Pharm Sin B.* 2015, *5*, 442–453. https://doi.org /10.1016/j.apsb.2015.07.003

4. De Melo, C. C.; Da Silva, C. C. P.; Pereira, C. C. S. S.; Rosa, P. C. P.; Ellena, J. Mechanochemistry Applied to Reformulation and Scale-up Production of

Ethionamide: Salt Selection and Solubility Enhancement. *Eur. J. Pharm. Sci.* 2016, *81*, 149–156. https://doi.org/10.1016/j.ejps.2015.10.007

5. Serajuddin, A. T. M. Salt Formation to Improve Drug Solubility. *Adv. Drug Deliv. Rev.* 2007, *59*, 603–616. https://doi.org/10.1016/j.addr.2007.05.010

6. Cruz-Cabeza, A. J. Acid–base Crystalline Complexes and the pKa Rule. *CrystEngComm* 2012, *14*, 6362–6365. https://doi.org/10.1039/c2ce26055g

7. Thomas Scior, T.; Raddatz, G.; Figueroa, R.; Roth, H. J.; Bisswanger, H. A. Molecular Modeling Study on Dapsone and Sulfonamides Comparing Structures and Properties with Respect to Anti-Leprosy Activity. *J. Mol. Model.* 1997, *3*, 332–337. https://doi.org/10.1007/s008940050047

8. Wozel, G. and Blasum, C. Dapsone in dermatology and beyond. *Arch. Dermatol. Res.* 2014, *306*, 103–124. https://doi.org/10.1007/s00403-013-1409-7

9. Zuidema, J.; Hilbers-Modderman, E.S.M. and Merkus, F.W.H.M. Clinical Pharmacokinetics of Dapsone. *Clin. Pharmacokinet*. 1986, *11*, 299–315. https://doi.org/10.2165/00003088-198611040-00003

10. Newton, D. W. and Kluza, R. B. pKa Values of Medicinal Compounds in Pharmacy Practice. *Drug Intell. Clin. Pharm.* 1978, *12*, 546–554. https://doi.org/10.1177/106002807801200906

11. Gaytán-Barrientos, N. S.; Morales-Morales, D.; Herrera-Ruiz, D.; Reyes-Martínez, R.; Rivera-Islas, J. Sulfonate salts of the therapeutic agent dapsone: 4-[(4-aminophenyl)sulfonyl]anilinium benzenesulfonate monohydrate and 4-[(4-aminophenyl)sulfonyl]anilinium methanesulfonate monohydrate. *Acta Cryst*. 2016, C72, 280–284. http://dx.doi.org/10.1107/S2053229616003284

12. Benahsene, A. H.; Bendjeddou, L.; Merazig, H. Crystal structure of bis-[bis-(4-azaniumylphenyl) sulfone] tetranitrate monohydrate. *Acta Cryst*. 2017, E73, 1721–1725. http://dx.doi.org/10.1107/S2056989017014803

13. Smith, G. and Wermuth, U. D. Proton-Transfer and Non-transfer Compounds of the Multi-purpose Drug Dapsone [4-(4-Aminophenylsulfonyl)aniline] with 3,5-Dinitrosalicylic Acid and 5-Nitroisophthalic Acid. *J. Chem. Crystallogr.* 2013, *43*, 664–670. http://dx.doi.org/10.1007/s10870-013-0470-6

14. Smith, G. and Wermuth, U. D. 4-(4-Aminophenylsulfonyl)anilinium toluene-4-sulfonate. *Acta Cryst.* 2014, E70, o37. http://dx.doi.org/10.1107/S1600536813033023

15. Deng, Z-P.; Huo, L-H.; Zhao, H.; Ga, S. A Co-Crystal Strategy to Tune the Supramolecular Patterns and Luminescent Properties: Ten Well-Designed Salts Assembled by Arenedisulfonic Acid with Diverse Diamines. *Cryst. Growth Des.* 2012, *12*, 3342−3355. https://dx.doi.org/10.1021/cg3004855

16. Braun, D. E.; Krüger, H.; Kahlenberg, V.; Griesser, U. J. Molecular Level Understanding of the Reversible Phase Transformation between Forms III and II of Dapsone. *Cryst. Growth Des.* 2017, *17*, 5054–5060. https://doi.org/10.1021/acs.cgd.7b01089

17. Braun, D. E.; Vickers, M.; Griesser, U. J. Dapsone Form V: A Late Appearing Thermodynamic Polymorph of a Pharmaceutical. *Mol. Pharm.* 2019, *16*, 3221–3236. http://dx.doi.org/10.1021/acs.molpharmaceut.9b00419

18. Lemmer, H.; Stieger, N.; Liebenberg, W.; Caira, M. R. Solvatomorphism of the Antibacterial Dapsone: X-ray Structures and Thermal Desolvation Kinetics. *Cryst. Growth Des.* 2012, *12*, 1683-1692. https://doi.org/10.1021/cg300019f

19. Jiang, L.; Huang, Y.; Zhang, Q.; He, H.; Xu, Y.; Mei, X. Preparation and Solid-State Characterization of Dapsone Drug−Drug Co-Crystals. *Cryst. Growth Des*. 2014, *14*, 4562–4573. https://doi.org/10.1021/cg500668a

20. Martins, I.; Martins, M.; Fernandes, A.; André, V.; Teresa Duarte, M. An insight into dapsone co-crystals: sulfones as participants in supramolecular interactions. *CrystEngComm*. 2013, *15*, 8173–8179. http://dx.doi.org/10.1039/c3ce41323c

21. Amidon, G. L.; Lennernäs, H.; Shah, V. P.; Crison, J. R. A Theoretical Basis for a Biopharmaceutic Drug Classification: The Correlation of in Vitro Drug Product Dissolution and in Vivo Bioavailability. *Pharm. Res.* 1995, *12*, 413–420

22. Bastin, R. J.; Bowker, M. J.; Slater, B. J. Salt Selection and Optimisation Procedures for Pharmaceutical New Chemical Entities. *Org. Proc. Res. Dev.* 2000, *4*, 427−435. https://doi.org/10.1021/op000018u

23. Benahsene, A. H.; Henchiri, R.; Ennaceur, N.; Carcelli, M.; Merazig, H.; Bendjeddou, L. Two Nitrates of Dapsone: New Candidates for Non-linear Optical

Materials. *J Mol Struct.* 2018, *1178*, 375–383. http://dx.doi.org/10.1016/j.molstruc.2018.10.011

24. Agilent, CrysAlis PRO, in: A. Technologies (Ed.). Yarnton, *England 2010*

25. Sheldrick, G. M. Crystal Structure Refinement with SHELXL. *Acta Cryst.* 2015, *C71*, 3–8. https://doi.org/10.1107/S2053229614024218

26. Macrae, C. F.; Bruno, I. J.; Chisholm, J. A.; Edgington, P. R.; McCabe, P.; Pidcock, E.; Rodriguez-Monge, L.; Taylor, R.; van de Streek, J.; Wood, P. A. Mercury CSD 2.0 - New Features for the Visualization and Investigation of Crystal Structures. *J. Appl. Cryst.* 2008, 41, 466-470. https://doi.org/10.1107/S0021889807067908

27. Allen, F. H. The Cambridge Structural Database : A Quarter of a Million Crystal Structures and Rising Research Papers. *Acta Cryst.* 2002, *B58*, 380–388. https://doi.org/10.1107/s0108768102003890

28. Sands, D. The Crystal Structure of Dimethyl Sulfone. *Zeitschrift für Kristallographie* 2010, *119*, 245–251. https://doi.org/10.1524/zkri.1964.119.16.245

29. Etter, M. C.; MacDonald, J. C.; Bernstein, J. Graph-set analysis of hydrogen-bond patterns in organic crystals. *Acta Cryst.* 1990, *B46*, 256–262. https://doi.org/10.1107/s0108768189012929

30. Robert M. Silverstein, Francis X. Webster, David Kiemle . *Spectrometric Identification of Organic Compounds*, 7th ed.; Wiley, Ed.; 2005

31. De Moura Oliveira, C. H.; De Melo, C. C.; Doriguetto, A. C. Sulfamethoxazole salts: crystal structures, conformations and solubility. *New J. Chem.* 2019, *43*, 10250–10258. https://doi.org/10.1039/c9nj00586b

32. Thompson, W. E.; Warren, R. J.; Eisdorfer, I. B.; Zarembo, J. E. Identification of Primary, Secondary, and Tertiary Pharmaceutical Amines by the Infrared Spectra of Their Salts. *J. Pharm. Sci.* 1965, *54*, 1819–1821. https://doi.org/10.1002/jps.2600541231

For Table of Contents Use Only

Investigating the Solubilities of the Nitrate and Isomorphous Bromide and Chloride Salts of Dapsone

Cristiane Cabral de Melo[*†,‡], *Monalisa Bitencourt* [†], *Charlane C. Correa* [§], *Antonio Carlos Doriguetto*[*†,‡]

†Faculty of Pharmaceutical Sciences and ‡Institute of Chemistry, Federal University of Alfenas, 37130-001, Alfenas-MG, Brazil

§Department of Chemistry, Federal University of Juiz de Fora, 36036-900, Juiz de Fora-MG, Brazil

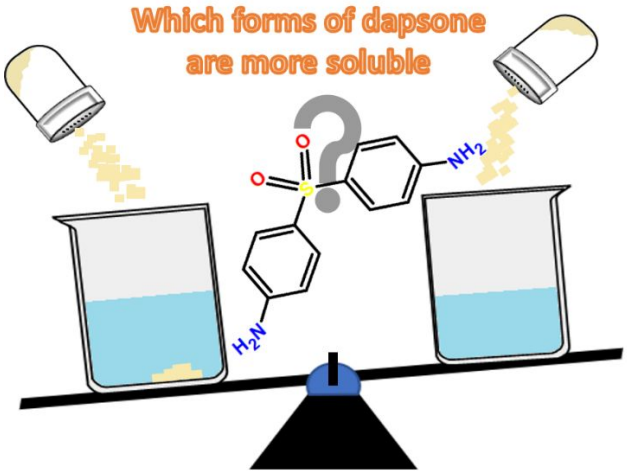

Pharmaceutical-acceptable salt forms of the anti-leprosy drug dapsone were prepared and characterized by X-ray diffraction (single and powder), FT-IR and thermal techniques. It was found that DDS chloride and DDS bromide are isomorphous compounds. The equilibrium solubility of the nitrate, chloride and bromide salts was investigated and compared to dapsone free base.